

# On Outage Performance of Terahertz Wireless Communication Systems

Jia Ye, *Student Member, IEEE*, Shuping Dang, *Member, IEEE*, Guoqing Ma, *Student Member, IEEE*, Osama Amin, *Senior Member, IEEE*, Basem Shihada, *Senior Member, IEEE*, and Mohamed-Slim Alouini, *Fellow, IEEE*

**Abstract**—To expedite research progress on terahertz (THz) communications, we analyze the outage performance of THz communication systems by a compound channel model in this paper. Different from existing models, the compound channel model incorporates the effects of spreading loss, molecular absorption loss, shadowing, and multi-path fading via a composite distribution. By using this model, we maintain an equilibrium of the outage performance analysis between mathematical tractability and the fidelity of realistic THz channels. Specifically, by utilizing the compound channel model, outage performance analysis can get rid of sophisticated case-specific channel modeling relying on field measurement and the ray-tracing assessment. To facilitate the application of the proposed channel model, we also design a maximum likelihood estimation (MLE) based channel parameter estimation approach for the compound channel model. The analytical results of outage performance by using the compound channel model are given in closed form and verified by numerical results.

**Index Terms**—Outage performance analysis, terahertz communications, compound/composite channel model, channel parameter estimation, gaseous molecular absorption.

## I. INTRODUCTION

NOVEL wireless communication applications pose ever-increasing requirements and challenges to the post fifth generation (post-5G) and sixth generation (6G) network design [1], among which the terabit-per-second (Tbps) wireless transmission is demanding and almost impossible by existing communication technologies. As foreseen in [2], both enhancing spectral efficiency (SE) and extending the available spectrum could be feasible solutions to the coming wireless capacity crisis with a set of preconditions. Different from non-orthogonal multiple access (NOMA) and index modulation (IM) that aim to enhance SE within a limited spectrum [3], [4], terahertz (THz) communication technology focuses on expanding the available spectrum to the frequency range between 0.1 THz and 10 THz [5]. In this way, a series of unprecedented wireless communication applications in the automotive

industry, indoor networking, indoor localization, environment monitoring, e-health, and defense will become realities within the next decade [6]–[8]. In addition to the advantage of tremendous spectrum, THz wireless communication systems are also miniature, energy-efficient, and secure [9]–[12]. Based on these unique advantages brought by THz communications, the THz frequency spectrum has been regarded as the last piece of radio frequency (RF) spectrum puzzle and the most promising option for high-speed and secure transmissions in the 6G era [5]. Since the hardware enabling technologies, e.g., the graphene-based plasmonic material, have been full-fledged, and the so-called ‘THz gap’ is gradually bridged [13], in recent years, researchers have paid particular attention to investigate the behavior of THz radios in both micro-scale and macro-scale networking contexts [14].

In the past, THz channels were jointly studied and regarded as an extension of millimeter-wave channels because of their shared high-frequency characterization [15]–[17]. However, through plenty of tests and studies, THz communications presents several crucial and unique features that are different from classic microwave communications below 95 gigahertz (GHz) and can yield significant impacts on wireless system modeling as well as future communication services. We summarize these features as follows:

- **Molecular absorption loss:** Because the radio frequencies of THz transmission windows are much higher than those of microwave communications, the corresponding wavelengths of THz radios are small and comparable to the scale of gaseous molecules. Such short wavelengths cause the molecular absorption phenomenon, especially when THz radios propagate through atmosphere and penetrate oxygen and water vapor [18]. In essence, the molecular absorption is caused by transforming the electromagnetic energy of the THz radio into the internal energy of the gaseous molecules in the propagation medium. Because the molecular absorption only occurs at resonance frequencies depending on the composition of the propagation medium for THz radios [19], the corresponding loss termed the *molecular absorption loss* makes THz band highly *frequency-selective*. The molecular absorption loss can be regarded as deterministic in most cases and is a distinguishing feature of THz wireless channels [20], [21].
- **Colored noise:** In addition, the molecular absorption causes not only extra path loss but also a special form

This work was supported by KAUST Office of Sponsored Research.

J. Ye, G. Ma, O. Amin, B. Shihada and M.-S. Alouini are with Computer, Electrical and Mathematical Science and Engineering Division, King Abdullah University of Science and Technology (KAUST), Thuwal 23955-6900, Kingdom of Saudi Arabia (e-mail: {shuping.dang, jia.ye, guoqing.ma osama.amin, basem.shihada, slim.alouini}@kaust.edu.sa).

S. Dang was with Computer, Electrical and Mathematical Science and Engineering Division, King Abdullah University of Science and Technology (KAUST), Thuwal 23955-6900, Kingdom of Saudi Arabia, is now with Department of Electrical and Electronic Engineering, University of Bristol, Bristol BS8 1UB, UK (e-mail: shuping.dang@bristol.ac.uk).

of noise termed the *molecular absorption noise*. Again, because the molecular absorption only occurs at specific resonance frequencies, the noise caused is *colored*. Also, it is obvious that the molecular absorption noise is self-induced and only appears during the transmitting phase [22]. The molecular absorption noise and the well-known background thermal noise jointly contribute to the detection errors at the THz radio receiver.

- **Limited transmission range:** In addition to the unique molecular absorption loss, the spreading loss of THz communications abiding the Friis' transmission law is inherently severe, since this loss is positively related to the transmission frequency [23]. Both losses constitute the harsh resultant propagation attenuation in the THz band and lead to limited direct transmission range normally within 10 m without utilizing directional antennas and beamforming techniques<sup>1</sup> [26]. This refers to the well-known 'THz wall' [18].
- **Dominant light-of-sight (LoS) path:** To mitigate the high path loss and ensure an adequate transmission range for THz communications, it is highly preferable to keep the LoS path between THz transmitter and receiver. Although THz radios have a better penetrating ability through non-transparent obstacles than optical radios [27], the LoS path still plays a dominant role for reliable THz communications and should be taken into consideration for THz channel modeling [5], [11], [21], [28].
- **Resolvable multi-path propagation links:** Because of the high frequency and wide bandwidth of the THz band, THz radios present quasi-optical behaviors, and the number of multi-path propagation links caused by reflection, scattering, and diffraction is quite limited compared to the microwave band below 95 GHz [23], [29]. These channel characteristics result in resolvable multi-path propagation links and are impactful in multi-path fading modeling for the THz band. The resolvable multi-path propagation can be regarded as a compromise between microwave communications and optical communications.
- **Dynamic shadowing:** Because of the small wavelength of the THz radio, it is fairly sensitive to human movement over the transmission link, which leads to the dynamic nature of shadowing for THz wireless channels [21], [30]–[32]. Therefore, shadowing should also be modeled as a stochastic factor in THz communications.
- **Distance-dependent transmission window:** The available spectrum and transmission windows in the THz band are highly dependent on the radio transmission distance [12]. This distance-dependent feature results in the space-frequency correlation for THz channel modeling and a high degree of sensitivity to the mobility of communi-

cation nodes when utilizing THz radios.

### A. Motivations and Contributions

Capturing all aforementioned features as well as other common electromagnetic effects of radios and carrying out outage performance of THz communications are not a trivial task. In particular, the trade-off between mathematical tractability and the fidelity of realistic THz channels must be carefully considered and made. For outage performance analysis, adopting an appropriate channel model maintaining a better equilibrium between mathematical tractability and the fidelity of realistic THz channels is the initial and the most important step. Motivated by the compound channel model proposed in [33], which is proved to be effective to capture the electromagnetic attributes of classic microwave channels and millimeter-wave channels [34]–[36], we propose the method to adopt and tailor the compound channel model to captures the THz channel behaviors and conduct a thorough study on the outage performance. The main contributions of the paper are summarized below.

- The tailored compound channel model is proposed considering only prominent peculiarities of THz channels yielding significant impacts on communication performance metrics, including the stochastic effects of spreading loss, molecular absorption loss, shadowing, and multi-path fading.
- All considered electromagnetic effects of THz radios are modeled on a holistic basis. The proposed tailored compound THz channel model is dominated by three easy-to-estimate free channel parameters, which is generic and can be modified to fit various application scenarios with different space-frequency state.
- The proposed compound channel model thus greatly facilitates the analysis and optimization for THz communications. The analytical results of outage performance of THz communication are given in a closed-form and are easy to scrutinize.
- To facilitate the application of the proposed channel model, we also employ the maximum likelihood estimation (MLE) method to design an estimation approach for the channel parameters.
- We employ Monte Carlo simulations to verify the derived analytical results and numerical reveal the outage performance of THz communications by adopting the tailored compound channel model.

The rest of this paper is structured as follows. We present the basics of the compound THz wireless channel model in Section II. The outage performance analysis of THz communications based on the tailored compound channel model is detailed in Section III. We further design the channel parameter estimation approach in Section IV. The numerical investigation of the tailored compound channel model and the numerical verification of the analytical results regarding outage performance by adopting the tailored compound channel model are given in Section V. Finally, we conclude the paper in Section VI.

<sup>1</sup>Although it has been demonstrated in [24] and [25] that the transmission range can be extended to 100 m and even thousands of meters for THz communications, a series of highly complicated physical layer (PHY) designs, including distance-aware transmission, ultra-massive multiple-input and multiple-output (MIMO) architectures, and intelligent surfaces, are required to work together to achieve this large transmission range. At present, these settings are cost-ineffective and thereby not feasible for practical implementations.

## II. TAILORED COMPOUND CHANNEL MODEL

### A. State of the Art

The THz band is expected to participate efficiently in the next generation wireless communication networks at different scales and in different application scenarios. In this paper, we mainly focus on the macro-scale and indoor THz networks. Indoor THz wireless communications can establish links between the transceivers through either LoS or non-LoS propagation path. Some studies consider deterministic setups and study models for both LoS and non-LoS propagation scenarios [37]–[39]. A comprehensive report of the latest progress on the indoor THz channel models can be found in [23].

For the LoS scenario, a small office is selected as a typical application scenario to measure the THz radios, and a ray-tracing simulator is invented according to the measured data [40]. The statistical parameters are considered and investigated for THz communication systems operating in the LoS scenario in [41], which are supported by experimental measurements. For non-LoS scenarios, researchers investigate reflection, diffraction, and scattering losses that are resulted from materials shape and surfaces roughness [42]. In a similar way, the equivalent path loss is developed using ray-tracing approach and verified by experimental results [43].

In [30], [44]–[46], the non-LoS components are investigated in depth, and the number of multi-path components are analyzed based on a specific density of reflecting objects and obstacles at each side of a rectangular room. In this way, stochastic multi-path channel models, frequency correlation functions, and power delay profiles are derived in [47]. Recently, statistical parameters for short-range LoS propagation are studied for a short range less than 20 cm and for THz band ranging from 275 GHz to 325 GHz [48]. The stochastic THz channel modeling method is in particular applied for kiosk applications in [49]. In a time-domain study proposing a model for causal THz wireless channels with a linear phase shift in [19], the authors derive a phase function that does not allow non-LoS radio arrivals before the LoS component.

### B. Channel Power Gain Model

Based on the brief literature review over the milestones presented above, there is still not a well-recognized channel model incorporating both determinate and stochastic radio propagation impairments. Specifically, the random variations on received radio power caused by dynamic shadowing and/or multi-path fading are always neglected. To facilitate our outage performance analysis, we introduce a mature channel modeling method for microwave wireless channels and tailor it to model the THz wireless channels in a compound manner [33], [50], [51].

Specifically, we consider a generic THz transmission scenario adopting a point-to-point (P2P) protocol and propose a compound channel model, where a single-antenna transmitter wants to communicate with a single-antenna receiver. The considered system model lays the foundation for future works studying more complicated communication scenarios, including multiple users or multiple antennas. The P2P transmission

distance between the THz transmitter and the THz receiver is denoted as  $d$ . Let the considered THz transmission bandwidth be  $B$  starting from the lower frequency limit  $f_L \geq 0.1$  THz and ending at the upper frequency limit  $f_U \leq 10$  THz<sup>2</sup>. That is,  $B = f_U - f_L$ . **In this paper, we attempt to construct the input-output relation of the power spectral densities (PSDs) for radio frequency  $f \in [f_L, f_U]$  when the compound channel model is tailored and adopted to incorporate the effects of molecular absorption.**

Following [14] and [20], this general relation can be expressed as

$$S_R(d, f) = \tilde{G}(d, f)S_T(f), \quad (1)$$

where  $S_T(f)$  and  $S_R(d, f)$  are the PSDs of the transmit and receive signals, respectively;  $\tilde{G}(d, f)$  is termed the *compound* channel power gain. The compound channel power gain  $\tilde{G}(d, f)$  is the emphasis of channel modeling in our work and can be further expanded as

$$\tilde{G}(d, f) = G_T(f)G_R(f)\tilde{g}(d, f), \quad (2)$$

where  $G_T(f)$  and  $G_R(f)$  is the transmitter and receiver gains characterizing the performance improvements brought by directional antenna architectures and beamforming techniques [14]<sup>3</sup>;  $\tilde{g}(d, f)$  is the internal channel power gain only related to the physical characteristics of the THz wireless channels *per se* and should be modeled as a random variable.

As suggested in [41], although the multi-path propagation links are resolvable in the THz band, the small-scale fading over THz wireless channels can still be modeled as Rayleigh, Rician, or Nakagami distributed depending on whether there is an LoS path between the THz transmitter and the THz receiver as well as the terrain over the propagation path. For generality, we adopt the Nakagami- $m$  distribution to model the small-scale fading in a compound manner<sup>4</sup>. Specifically, different from most existing works starting the THz channel modeling from the determinate molecular absorption attenuation derived by the Beer-Lambert law, we inspect the THz channel from a stochastic and compound perspective. In this way, the determinate and stochastic effects of spreading loss, molecular absorption loss, shadowing, and multi-path fading can be integrated into one single and stochastic entity, which can provide much better mathematical tractability [33].

By adopting the Nakagami- $m$  channel model, the internal channel power gain  $\tilde{g}(d, f)$ , i.e., the square of the channel

<sup>2</sup>Note that, for practical THz communication systems, only a small portion of the entire THz spectrum will be used to transmit data by a single THz transceiver pair, due to the hardware restrictions. The used spectrum might refer to a single or multiple transmission windows. Here, we define the lower and upper limits of the THz spectrum just for prescribing a limit to the scope of the discussion in this paper. This does not imply that the entire THz spectrum can be utilized by a single THz transceiver pair.

<sup>3</sup>We do not specify the antenna architectures and beamforming techniques in this work, but consider the general THz communication scenarios. In other words, the proposed channel model and derived results in the following fit for different THz communication scenarios by changing the values of transmitting/receiving gain for various antenna architectures and the beamforming techniques.

<sup>4</sup>This is because the Nakagami- $m$  distribution is general and can reveal the signal propagation environment with a higher degree of freedom. Meanwhile, the Nakagami- $m$  fading can be easily reduced to both Rayleigh fading composed of NLoS paths, and Rician fading considering both LoS and NLoS paths, by alternating the model parameters [52].

response envelope, should be modeled as gamma distributed with cumulative distribution function (CDF) and probability density function (PDF) given by [52]

$$F_{\tilde{g}}(d, f, x) = \mathbb{P}\{\tilde{g}(d, f) < x\} = \frac{\gamma\left(m(d, f), \frac{m(d, f)}{\tilde{\Omega}(d, f)}x\right)}{\Gamma(m(d, f))} \quad (3a)$$

$$f_{\tilde{g}}(d, f, x) = \frac{m(d, f)^{m(d, f)} x^{m(d, f)-1}}{\Gamma(m(d, f)) \tilde{\Omega}(d, f)^{m(d, f)}} \exp\left(-\frac{m(d, f)}{\tilde{\Omega}(d, f)}x\right), \quad (3b)$$

where  $\mathbb{P}\{\cdot\}$  denotes the probability of the random event enclosed;  $\Gamma(\cdot)$  and  $\gamma(\cdot, \cdot)$  are the gamma function and the lower incomplete gamma function, respectively;  $m(d, f) \geq 0$  is a distance- and frequency-dependent fading figure characterizing the nature of the small-scale fading for a given propagation environment;  $\tilde{\Omega}(d, f)$  is the shadowing factor. Comparing (3) to the standard form of the Gamma distribution, it is obvious that the shape and scale parameters are given by  $\kappa_{\tilde{g}}(d, f) = m(d, f)$  and  $\theta_{\tilde{g}}(d, f) = \tilde{\Omega}(d, f)/m(d, f)$ , respectively.

According to [33], the shadowing factor  $\tilde{\Omega}(d, f)$  can also be modeled as a Gamma distributed random variable for THz wireless channels, because of the dynamic shadowing nature in the THz band. Based on the detailed derivations given in [33], the CDF and PDF pertaining to  $\tilde{\Omega}(d, f)$  are given as

$$F_{\tilde{\Omega}}(d, f, x) = \frac{\gamma\left(\frac{1}{\xi_1(d, f)}, \frac{x}{\Psi(d, f)\xi_1(d, f)\xi_2(d, f)}\right)}{\Gamma\left(\frac{1}{\xi_1(d, f)}\right)}, \quad (4a)$$

$$f_{\tilde{\Omega}}(d, f, x) = \frac{x^{\frac{1}{\xi_1(d, f)}-1} \exp\left(-\frac{x}{\Psi(d, f)\xi_1(d, f)\xi_2(d, f)}\right)}{\Gamma\left(\frac{1}{\xi_1(d, f)}\right) [\Psi(d, f)\xi_1(d, f)\xi_2(d, f)]^{\frac{1}{\xi_1(d, f)}}}, \quad (4b)$$

where  $\xi_1(d, f) = \exp(\sigma(d, f)^2) - 1$ ,  $\xi_2(d, f) = \exp(\sigma(d, f)^2/2)$ ,  $\sigma(d, f) \geq 0$  is the shadowing figure that characterizes the severity of shadowing and is related to the material of obstacle;  $\Psi(d, f)$  is the path attenuation factor related to both spreading loss and molecular absorption loss, which are determinate and dependent on transmission distance and radio frequency. Similarly, comparing (4) to the standard form of the Gamma distribution, we can find the shape and scale parameters to be  $\kappa_{\tilde{\Omega}}(d, f) = \frac{1}{\xi_1(d, f)}$  and  $\theta_{\tilde{\Omega}}(d, f) = \Psi(d, f)\xi_1(d, f)\xi_2(d, f)$ , respectively.

According to the Friis transmission law and the Beer-Lambert law, we can express the path attenuation factor  $\Psi(d, f)$  as [37]

$$\Psi(d, f) = \left(\frac{c}{4\pi fd}\right)^\alpha \underbrace{\exp(-k_A(f)d)}_{\psi(d, f)}, \quad (5)$$

where  $c$  is the speed of light;  $\alpha \in [2, 7]$  is the spreading loss exponent depending on terrain<sup>5</sup>;  $k_A(f)$  is the medium absorption coefficient that is related to the radio frequency,

<sup>5</sup> $\alpha = 2$  is for free space transmission;  $\alpha \in [4, 6]$  corresponds to indoor transmission;  $\alpha > 6$  is normally for complex electromagnetic environments with obstruction [53].

the propagation medium composition, the equivalent medium temperature in Kelvin, and the equivalent medium pressure<sup>6</sup>;  $\psi(d, f) = \exp(-k_A(f)d)$  is called the medium transmittance, which captures the impact of molecular absorption on internal channel power gain.

From the above description, it is clear that the internal channel power gain  $\tilde{g}(d, f)$  is a conditioned variable on the shadowing factor  $\tilde{\Omega}(d, f)$  that is latent in the CDF and PDF of  $\tilde{g}(d, f)$ . The shadowing factor  $\tilde{\Omega}(d, f)$  is also a random variable dominated by the path attenuation factor and the shadowing figure in its CDF and PDF. The holistic procedure of compound channel modeling can be pictorially illustrated in Fig. 1 for clarity.

**Remark:** There are several advantages to adopt the compound channel model for THz communications. First, from the modeling perspective, researchers can evade the measurements of geometrical and material parameters for a specific transmission environment, which normally involve sophisticated procedures and are time-consuming. This is particularly helpful, as the estimation of medium absorption coefficients that requires detailed physical modeling in the ray-tracing approach can be circumvented. Researchers only need to inspect the input and output powers and estimate the three free channel parameters, i.e.,  $\psi(d, f)$ ,  $\sigma(d, f)$ , and  $m(d, f)$ . Second, from the performance analytical perspective, classic analytical methodologies built for microwave communication systems can be similarly transferred to THz communication systems, when the compound THz channel model is in use.

### C. Noise Model

The molecular absorption causes not only extra path loss but also additional noise called the molecular absorption noise. There are numerous ways to model the molecular absorption noise [20], [22], [37]. There is still neither a consensus reached nor a widely acknowledged model for the molecular absorption noise, because the essential nature of this noise has not been fully revealed by physics [22]. In fact, the molecular absorption noise is an additional noise source caused by transmission *per se*, which is dependent on the frequency and the communication distance between the transmitter and the receiver. A detailed discussion on molecular noise is provided in [22], as well as the core model of the molecular absorption noise models, which is widely adopted in existing reference [54]–[57] with some variations regarding how to take into account the spreading loss and the antenna aperture. Relying on these references and justified in [20], [31], we give the molecular absorption noise model given as follows, which captures the prominent features of the molecular absorption noise and is easy to analyze.

This noise model is dependent on transmission distance, radio frequency, and the PSD of the transmit signal. The PSD of the molecular absorption noise can be expressed as

$$N_A(d, f) = G_T(f)G_R(f)S_T(f) \left(\frac{c}{4\pi fd}\right)^\alpha (1 - \psi(d, f)). \quad (6)$$

<sup>6</sup>The formulation of  $k_A(f)$  is highly complex and has been detailed in [37] by a series of physical laws.

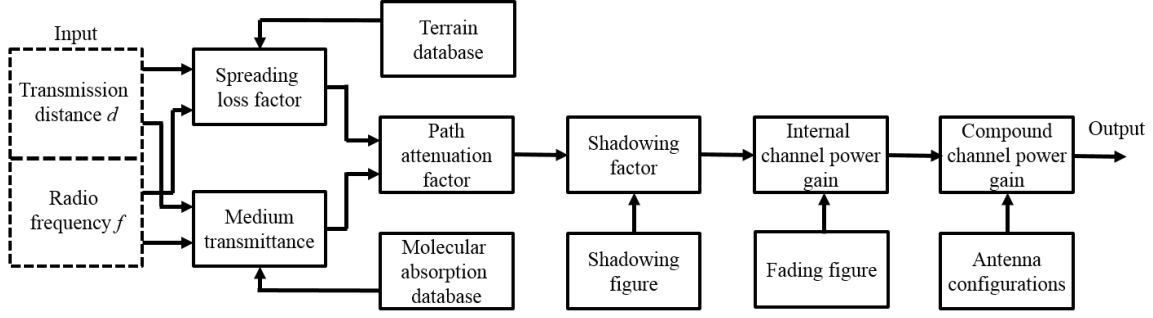


Fig. 1: Holistic procedure of compound channel modeling, integrating spreading loss, molecular absorption loss, shadowing, multi-path fading, and antenna configurations.

Meanwhile, the background thermal noise in the THz band behaves similarly as in the microwave bands and is white. The PSD of the thermal noise is given by  $N_0 = k_B T$ , where  $k_B$  is the Boltzmann constant, and  $T$  is the equivalent medium temperature in Kelvin.

As a result of the additivity of noises, the resultant noise PSD in the THz band can be determined by

$$N(d, f) = N_A(d, f) + N_0. \quad (7)$$

By observing (6), an apparent advantage of the noise model is that the only parameter required to be estimated is  $\psi(d, f)$ , because  $d$ ,  $f$ , and  $\alpha$  are normally known by practical communication systems, especially when the network scale is small [58]. As  $\psi(d, f)$  needs to be estimated when modeling the compound channel power gain, the noise model can be easily obtained as a by-product of modeling the compound channel power gain. That is, no extra parameter estimation is required for the noise model in the THz band when adopting the noise model formulated in (7).

### III. OUTAGE PERFORMANCE ANALYSIS

#### A. State of the Art

There are a couple of works laying the foundation for the outage performance analysis of THz communication systems. The authors in [59] studied the outage performance of THz communication system under the Rayleigh fading channel model and the path loss model proposed in [60], which is only determined by the transmission distance. In [61], the closed-form expressions for the outage probability of a THz relaying system were derived considering the generalized Gamma distribution channel and misalignment fading. In addition to the misalignment fading, the authors in [62] studied the impact of the phase noise on THz wireless systems, while the fading channel is assumed to follow the Nakagami-m distribution. Moreover, in [63], the small-scale fading is assumed to follow the Rician distribution, while the molecular attenuation is assumed to be determined by the transmission frequency and communication distance when evaluating the performance of the initial access procedure in THz communication systems.

However, the assumed channel models in the abovementioned literature only capture partial properties of THz communications or target for a special communication environment. The most recent work [64] studied the outage performance of

single-input and multiple-output (SIMO) THz communication system adopting the maximal ratio combining (MRC) scheme under the assumption that the transmitted signals experience fluctuating two-ray fading [65]. No evidence shows the fluctuating two-ray fading model can capture the full properties of the THz channel, notwithstanding. To the best of the authors' knowledge, there is still no work to analyze the outage performance of THz communication systems under a compound and general THz channel model with adjustable parameters for various propagation environments, which incorporate both determinate and stochastic radio propagation impairments. To bridge the gap of performance analysis for THz communications systems, we derive the exact and asymptotic closed-form expressions for the outage probability under the proposed compound channel in this section.

#### B. Outage Probability

To analyze THz wireless channels from a compound perspective, we can determine the unconditional PDF of the internal channel power gain  $\tilde{g}(d, f)$  by marginalizing over the latent shadowing factor  $\tilde{\Omega}(d, f)$ , which yields

$$\begin{aligned} \phi(d, f, x) &= \int_0^\infty f_{\tilde{g}}(d, f, x|y) f_{\tilde{\Omega}}(d, f, y) dy \\ &= C_1(d, f) x^{C_2(d, f)} K_{C_3(d, f)} \left( C_4(d, f) x^{\frac{1}{2}} \right), \end{aligned} \quad (8)$$

where  $K_v(\cdot)$  represents the  $v$ th-order modified Bessel function of the second kind;  $C_1(d, f) \sim C_4(d, f)$  are distance- and frequency-dependent constant coefficients that are explicitly given by

$$C_1(d, f) = \frac{2 \left[ \frac{m(d, f) \left( \frac{4\pi df}{c} \right)^\alpha}{\psi(d, f) \xi_1(d, f) \xi_2(d, f)} \right]^{\frac{1}{2} \left( \frac{1}{\xi_1(d, f)} + m(d, f) \right)}}{\Gamma(m(d, f)) \Gamma \left( \frac{1}{\xi_1(d, f)} \right)}, \quad (9a)$$

$$C_2(d, f) = \frac{1}{2} \left( \frac{1}{\xi_1(d, f)} + m(d, f) \right) - 1, \quad (9b)$$

$$C_3(d, f) = \frac{1}{\xi_1(d, f)} - m(d, f), \quad (9c)$$

and

$$C_4(d, f) = 2 \left[ \frac{m(d, f) \left( \frac{4\pi df}{c} \right)^\alpha}{\psi(d, f) (\xi_1(d, f)) \xi_2(d, f)} \right]^{\frac{1}{2}}. \quad (9d)$$

According to the relation between CDF and PDF, we can determine the unconditional CDF of the internal channel power gain  $\tilde{g}(d, f)$  as

$$\begin{aligned}\Phi(d, f, x) &= \int_0^x \phi(d, f, t) dt \\ &= D_3(d, f)x^{D_1(d, f)} {}_1F_2(D_1(d, f); D_5(d, f); D_0(d, f)x) \\ &\quad + D_4(d, f)x^{D_2(d, f)} {}_1F_2(D_4(d, f); D_6(d, f); D_0(d, f)x),\end{aligned}\quad (10)$$

where  ${}_pF_q(\mathbf{a}; \mathbf{b}; \cdot)$  denotes the generalized hypergeometric function,  $D_0(d, f) = \left(\frac{C_4(d, f)}{2}\right)^2$ ,  $D_1(d, f) = 1 + C_2(d, f) - \frac{C_3(d, f)}{2}$ ,  $D_2(d, f) = 1 + C_2(d, f) + \frac{C_3(d, f)}{2}$ ,  $D_3(d, f) = \frac{C_1(d, f)2^{C_3(d, f)-1}\Gamma(C_3(d, f))}{C_4(d, f)^{C_3(d, f)}D_1(d, f)}$ ,  $D_4(d, f) = \frac{C_1(d, f)C_4(d, f)^{C_3(d, f)}\Gamma(-C_3(d, f))}{2^{C_3(d, f)+1}D_2(d, f)}$ ,  $D_5(d, f) = [1 - C_3(d, f), 2 + C_2(d, f) - \frac{C_3(d, f)}{2}]$ , and  $D_6(d, f) = [2 + C_2(d, f) + \frac{C_3(d, f)}{2}, 1 + C_3(d, f)]$ .

Considering the high-frequency band used in THz communications, most communication scenarios only occupy a small bandwidth, especially for single-user cases. If the bandwidth is small enough, the channel can be regarded as frequency-nonselective and appears to be locally flat [66], [67]. Specifically, we assume that the number of available transmission windows is denoted as  $w(d)$ , which is a distance-dependent variable, and the available bandwidth of each window is denoted as  $B_i(d)$ . In general, we have  $\sum_{i=1}^{w(d)} B_i(d) \leq B$ . Assuming there is a critical distance  $d_C$  (experimental measurements show  $d_C \approx 1$  m when propagating through the atmosphere [12]), when  $d < d_C$ , the molecular absorption is not obvious, and thereby the number of transmission windows  $w(d)$  is small, which yields a relatively large bandwidth  $B_i(d)$  ranging from  $f_{L:i}(d)$  to  $f_{U:i}(d)$ ,  $\forall i \in \{1, 2, \dots, w(d)\}$ , and a frequency-selective model of each window. On the other hand, when  $d \geq d_C$ , the molecular absorption becomes severe at a large number of resonance frequencies throughout the entire spectrum  $[f_L, f_U]$ , and the number of transmission windows goes large accordingly<sup>7</sup>. In this case, the channel corresponding to each transmission window with bandwidth  $B_i(d)$  and center frequency  $f_{T:i}(d) = (f_{L:i}(d) + f_{U:i}(d))/2$  can be regarded as frequency-flat. As a direct consequence of this distance-dependent nature, the THz wireless channels can be classified into two categories depending on  $d < d_C$  (for micro-scale THz networks) and  $d \geq d_C$  (for macro-scale THz networks). Considering that THz networks are supposed to be deployed in the 6G era for supporting indoor and industrial application scenarios with about 5-10 m radio propagation distances, we only analyze the outage performance of micro-scale THz networks in the following, in which the THz channels within

<sup>7</sup>It is worth noting that a particular type of molecule does not confine the molecular absorption at a single resonance frequency, but spreads the molecular absorption over a range of resonance frequencies [37].

transmission windows are approximately flat<sup>8</sup>

Considering only the  $i$ th transmission window that is assumed to be flat, the channel capacity can be determined by the Shannon–Hartley theorem to be

$$\begin{aligned}C_i(d) &= B_i(d) \log_2 \left( 1 + \frac{S_R(d, f_{T:i}(d))}{N(d, f_{T:i}(d))} \right) \\ &= B_i(d) \log_2 \left( 1 + \frac{\Xi(d, f_{T:i}(d))\tilde{g}(d, f_{T:i}(d))}{N(d, f_{T:i}(d))} \right),\end{aligned}\quad (11)$$

where  $\Xi(d, f_{T:i}(d)) = G_T(d, f_{T:i}(d))G_R(f_{T:i}(d))S_T(d, f_{T:i}(d))$ . Denoting the data size, which is defined as the number of bits required to be transmitted, over the  $i$ th transmission window as  $\Theta_i$ , we can calculate the transmission latency to be

$$D_i(d) = \Theta_i / C_i(d). \quad (12)$$

More specifically, the transmitted data is composed of multiple packets, while all packets have the same length of  $L$  bits. In other words,  $\Theta_i = N_i L$ , where  $N_i$  denotes the number of packets, which follows a Poisson distribution with an average rate of  $\lambda_p$  packets<sup>9</sup> characterized by the probability mass function (PMF) [68]:

$$\mathbb{P}\{N_i = N\} = \frac{\lambda_p^N e^{-\lambda_p}}{N!}. \quad (13)$$

In this way, we can define the outage probability of a THz communication system utilizing the  $i$ th transmission window as

$$P_{\text{out}:i}(\varepsilon) = \mathbb{P}\{D_i(d) > \varepsilon\}, \quad (14)$$

where  $\varepsilon$  is a preset outage threshold depending on the system specifications and service demands.

Substituting (11) and (12) into (14), the outage probability of a THz communication system utilizing the  $i$ th transmission window can be reduced in (15). It should be noted that we consider the general case here with a random transmitted packet size. Once the packet size  $\Theta_i$  is fixed over the  $i$ th transmission window, the outage probability can be further simplified as

$$P_{\text{out}:i}(\varepsilon) = \Phi \left( d, f_{T:i}(d), \frac{\left( 2^{\frac{\Theta_i}{B_i(d)\varepsilon}} - 1 \right) N(d, f_{T:i}(d))}{\Xi(d, f_{T:i}(d))} \right). \quad (16)$$

### C. Asymptotic Outage Probability

To illustrate the relation among outage performance and a set of system parameters and thereby provide profound insights, we present the asymptotic analysis of outage performance in this subsection.

<sup>8</sup>The assumption is ideal in some aspects, and the considered scenario in this work may be thought of as an ideal case, but it brings simplicity and mathematical tractability, which are expected to considerably facilitate advanced analyses and system designs for THz communication systems. We intend to bring a general picture for the performance of THz communication systems by conducting analysis under the assumption..

<sup>9</sup>In this work, we omit the estimation details for the average rate  $\lambda_p$  here since it is not the focus of this work. We assume the average rate  $\lambda_p$  to be well estimated and known at the receiver.

$$\begin{aligned}
P_{\text{out};i}(\varepsilon) &= \mathbb{P} \left\{ \Theta_i \left( B_i(d) \log_2 \left( 1 + \frac{\Xi(d, f_{T:i}(d)) \tilde{g}(d, f_{T:i}(d))}{N(d, f_{T:i}(d))} \right) \right)^{-1} > \varepsilon \right\} \\
&= \sum_{N=0}^{\infty} \mathbb{P} \left\{ \frac{\left( 2^{\frac{NL}{B_i(d)\varepsilon}} - 1 \right) N(d, f_{T:i}(d))}{\Xi(d, f_{T:i}(d))} \tilde{g}(d, f_{T:i}(d)) | N_i = N \right\} \mathbb{P} \{ N_i = N \} \\
&= \sum_{N=0}^{\infty} \frac{\lambda_p^N e^{-\lambda_p}}{N!} \Phi \left( d, f_{T:i}(d), \frac{\left( 2^{\frac{NL}{B_i(d)\varepsilon}} - 1 \right) N(d, f_{T:i}(d))}{\Xi(d, f_{T:i}(d))} \right)
\end{aligned} \tag{15}$$

1)  $\Theta_i \rightarrow 0$ : Firstly, we assume that the number of bits required to be transmitted goes to zero, which indicates  $\Theta_i \rightarrow 0$ . This assumption corresponds to the cases where the length of each packet goes to zero, i.e.,  $L \rightarrow 0$ , or the average arrival rate goes to zero, i.e.,  $\lambda_p \rightarrow 0$ . Observing the CDF function defined in (10), we can find that the third parameter goes to zero, that is,  $\frac{\left( 2^{\frac{\Theta_i}{B_i(d)\varepsilon}} - 1 \right) N(d, f_{T:i}(d))}{\Xi(d, f_{T:i}(d))} \rightarrow 0$ . As referred to [69], the generalized hypergeometric function  ${}_1F_2(a; b_1, b_2; \cdot)$  can be expanded by generalized hypergeometric series as

$${}_1F_2(a; b_1, b_2; x) = \sum_{k=0}^{\infty} \frac{(a)_k x^k}{(b_1)_k (b_2)_k k!}, \tag{17}$$

which can be approximated to be

$${}_1F_2(a; b_1, b_2; x) \approx 1 + \frac{a_1 x}{b_1 b_2}, \tag{18}$$

by only keeping the first two terms when  $x \rightarrow 0$ . Accordingly, the asymptotic outage probability can be derived by adopting (18) into (16) to be (19) shown on the top of next page, where  $\chi = \frac{D_0(d, f_{T:i}(d)) N(d, f_{T:i}(d))}{\Xi(d, f_{T:i}(d))}$ .

2)  $S_T(d, f_{T:i}(d)) \rightarrow \infty$ : As given in Section II.C, the received noise power increases as the transmitting PSD increases, which motivates us to investigate the performance when the PSD of the transmit signals goes to infinity, that is,  $S_T(d, f_{T:i}(d)) \rightarrow \infty$ . The third parameter in the CDF function defined in (10) can be rewritten through substituting  $N(d, f_{T:i}(d))$  by the expression given in (7) to be (20) shown on the top of next page. By letting  $S_T(d, f_{T:i}(d)) \rightarrow \infty$ , we have  $\Xi(d, f_{T:i}(d)) \rightarrow \infty$ , and the second term in (20) goes to zero, that is,  $\frac{\left( 2^{\frac{\Theta_i}{B_i(d)\varepsilon}} - 1 \right) N_0}{\Xi(d, f_{T:i}(d))} \rightarrow 0$ . Therefore, the third parameter in (10) can be asymptotically written as

$$\begin{aligned}
&\frac{\left( 2^{\frac{\Theta_i}{B_i(d)\varepsilon}} - 1 \right) N(d, f_{T:i}(d))}{\Xi(d, f_{T:i}(d))} \\
&\rightarrow \left( 2^{\frac{\Theta_i}{B_i(d)\varepsilon}} - 1 \right) \left( \frac{c}{4\pi f_{T:i}(d)d} \right)^\alpha (1 - \psi(d, f_{T:i}(d))).
\end{aligned} \tag{21}$$

We can tell from (21) that the asymptotic outage probability as  $S_T(d, f_{T:i}(d)) \rightarrow \infty$  does not depend on the transmitting PSD anymore. In other words, the outage probability approaches a fixed floor as the transmitting PSD increases.

#### IV. ESTIMATION OF FREE CHANNEL PARAMETERS

From (8) and (10), it is obvious that for a given space-frequency state  $(d, f)$  in a specific propagation environment, the distribution of the internal channel power gain is determined by only three free parameters:  $\psi(d, f)$ ,  $\sigma(d, f)$ , and  $m(d, f)$ , which characterize the severity of molecular absorption loss, shadowing, and multi-path fading, respectively. As long as these three free parameters can be estimated for a sufficiently large set of space-frequency states  $(d, f)$  using empirical data, the THz wireless channel model can be constructed and analyzed on a compound basis by (2). In this section, we employ the MLE method to estimate these three free channel parameters.

##### A. MLE Problem Formulation and Decomposition

As the MLE method has been proven to be feasible for most parameter estimation problems and a dominant means of statistical inference [70], we formulate the channel parameter MLE problem and then solve it to yield the estimates. First of all, it should be noted that the estimation problem is not for three parameters, but in fact three sets of parameters  $\{\psi(d, f)\}$ ,  $\{\sigma(d, f)\}$ , and  $\{m(d, f)\}$  for a two-dimensional continuous and unbounded state space  $\{(d, f)\}$ . In practice, it is not possible to estimate the parameters in an unbounded and continuous manner. In this regard, the free parameter estimation can only be carried out over a discrete and bounded grid consisting of finite space-frequency states. The representative values of transmission distance  $d$  and radio frequency  $f$  are selected from shrinking finite subsets  $\mathcal{D}$  and  $\mathcal{F}$ , respectively.

Assume that the channel power gains corresponding to different space-frequency states are mutually independent. Based on this assumption, we can decouple the holistic channel parameter estimation problem to  $|\mathcal{D}| \times |\mathcal{F}|$  independent sub-problems pertaining to all selected space-frequency states. By this simplification, for a specific space-frequency state  $(d, f)$ ,  $d \in \mathcal{D}$  and  $f \in \mathcal{F}$ , we can measure  $S$  independent random realization samples (a.k.a. the empirical data) of the internal channel power gain  $\tilde{g}(d, f)$ , denoted as  $\{g_s(d, f)\}$ ,  $s = 1, 2, \dots, S$ . Because  $\tilde{g}(d, f)$  is a continuous random variable, we have  $g_1(d, f) \neq g_2(d, f) \neq \dots \neq g_S(d, f)$ . Subsequently, we can utilize these  $S$  random realization samples and employ the MLE method to estimate  $\psi(d, f)$ ,  $\sigma(d, f)$ , and  $m(d, f)$  for a specific space-frequency state  $(d, f)$ .

$$\begin{aligned}
P_{\text{out};i}^A(\varepsilon) &= D_3(d, f_{T:i}(d)) \left( \chi \left( 2^{\frac{\Theta_i}{B_i(d)\varepsilon}} - 1 \right) \right)^{D_1(d, f_{T:i}(d))} \left( 1 + \frac{D_1(d, f_{T:i}(d)) \chi \left( 2^{\frac{\Theta_i}{B_i(d)\varepsilon}} - 1 \right)}{(1 - C_3(d, f_{T:i}(d))) \left( 2 + C_2(d, f_{T:i}(d)) - \frac{C_3(d, f_{T:i}(d))}{2} \right)} \right) \\
&\quad + D_4(d, f_{T:i}(d)) \left( \chi \left( 2^{\frac{\Theta_i}{B_i(d)\varepsilon}} - 1 \right) \right)^{D_2(d, f_{T:i}(d))} \left( 1 + \frac{D_4(d, f_{T:i}(d)) \chi \left( 2^{\frac{\Theta_i}{B_i(d)\varepsilon}} - 1 \right)}{\left( 2 + C_2(d, f_{T:i}(d)) + \frac{C_3(d, f_{T:i}(d))}{2} \right) (1 + C_3(d, f_{T:i}(d)))} \right)
\end{aligned} \tag{19}$$

$$\begin{aligned}
\frac{\left( 2^{\frac{\Theta_i}{B_i(d)\varepsilon}} - 1 \right) N(d, f_{T:i}(d))}{\Xi(d, f_{T:i}(d))} &= \frac{\left( 2^{\frac{\Theta_i}{B_i(d)\varepsilon}} - 1 \right) \left( \Xi(d, f_{T:i}(d)) \left( \frac{c}{4\pi f_{T:i}(d)d} \right)^\alpha (1 - \psi(d, f_{T:i}(d))) + N_0 \right)}{\Xi(d, f_{T:i}(d))} \\
&= \left( 2^{\frac{\Theta_i}{B_i(d)\varepsilon}} - 1 \right) \left( \frac{c}{4\pi f_{T:i}(d)d} \right)^\alpha (1 - \psi(d, f_{T:i}(d))) + \frac{\left( 2^{\frac{\Theta_i}{B_i(d)\varepsilon}} - 1 \right) N_0}{\Xi(d, f_{T:i}(d))}
\end{aligned} \tag{20}$$

In particular, because of the independence among all  $S$  random samples, we can construct the MLE function as follows for a specific space-frequency state  $(d, f)$ :

$$\begin{aligned}
&\ell(\psi(d, f), \sigma(d, f), m(d, f) | g_1(d, f), \dots, g_S(d, f)) \\
&= \log \left( \prod_{s=1}^S \phi(d, f, g_s(d, f); \{\psi(d, f), \sigma(d, f), m(d, f)\}) \right),
\end{aligned} \tag{22}$$

where  $\log(\cdot)$  denotes the natural logarithmic function and is introduced to facilitate the processing and manipulation of the MLE function. Because for each sub-problem,  $d$  and  $f$  are fixed, we can simplify the denotation in (22) to be  $\ell(\psi, \sigma, m) = \log \left( \prod_{s=1}^S \phi_s(\psi, \sigma, m) \right)$  for brevity. As a result, we obtain the estimated channel parameters  $\hat{\psi}(d, f)$ ,  $\hat{\sigma}(d, f)$ , and  $\hat{m}(d, f)$  according to the following MLE criterion:

$$\begin{aligned}
&\{\hat{\psi}(d, f), \hat{\sigma}(d, f), \hat{m}(d, f)\} = \arg \max_{\psi, \sigma, m} \{\ell(\psi, \sigma, m)\} \\
&= \arg \max_{\psi, \sigma, m} \left\{ \sum_{s=1}^S \log(\phi(\psi, \sigma, m)) \right\}, \\
&\text{s.t., } 0 < \psi \leq 1, \sigma \geq 0, m \geq 0.
\end{aligned} \tag{23}$$

### B. Solutions to the Likelihood Equation Set

To ease the following analysis, we denote  $\lambda = (4\pi f d/c)^\alpha$ ,  $\varsigma = \exp(\sigma^2/2)$  and thereby have  $\exp(\sigma^2) - 1 = \varsigma^2 - 1$ . By (8) and (9), the MLE function can be explicitly rewritten and simplified in (24). From (24), one should note that since  $\Psi(d, f)$  is small in the THz band,  $g_s$  is a small value, which leads to an extremely large negative value of  $\ell(\psi, \sigma, m)$  when  $S$  goes high. In most cases, such a large value exceeds the processing and/or storage capability of numerical computing programs, e.g., MATLAB. As a result, either an error message or inaccurate solutions will be returned. Therefore, to mitigate this problem, we split the original MLE problem of (23) into  $S$  sub-MLE problem pertaining to each random realization sample:

$$\begin{aligned}
&\{\hat{\psi}_s(d, f), \hat{\sigma}_s(d, f), \hat{m}_s(d, f)\} = \arg \max_{\psi, \sigma, m} \{\log(\phi_s(\psi, \sigma, m))\}, \\
&\text{s.t., } 0 < \psi \leq 1, \sigma \geq 0, m \geq 0, 1 \leq s \leq S.
\end{aligned} \tag{25}$$

To solve this problem (25), we propose to use the Barrier method [71]. By this method, the reduced optimization problem should first be approximated as a non-constrained problem to reduce the computational complexity. The non-constrained problem can be easily solved by existing optimization algorithms, e.g., gradient descent, the Newton-Raphson method, and the conjugate gradient method. Taking the advantages of the fast convergence and low consumption of memory, we adopt the conjugate gradient method to solve the reduced non-constrained problem. Define an alternative objective function as  $\nu(\psi, \sigma, m)$  as follows:

$$\nu(\psi, \sigma, m) = -\log(\phi_s(\psi, \sigma, m)) + \Lambda(\psi, \sigma, m)/\tau, \tag{26}$$

where  $\Lambda(\psi, \sigma, m) = -(\log(\psi) + \log(1-\psi) + \log(\sigma) + \log(m))$  and  $\tau > 0$  is a process control parameter. Thus, the reduced channel parameter estimation problem formulated in (25) can be approximated by the following problem

$$\{\hat{\psi}_s(d, f), \hat{\sigma}_s(d, f), \hat{m}_s(d, f)\} \approx \arg \min_{\psi, \sigma, m} \{\nu(\psi, \sigma, m)\}. \tag{27}$$

The accuracy of the above approximation can be controlled by the process control parameter  $\tau$ . A larger  $\tau$  will lead to a more accurate approximate results, and vice versa. The approximation process introduced above is presented in Algorithm 1.

Then, we average all  $S$  estimated parameters taking  $g_s(d, f)$  as weights and obtain the final estimated parameters to be

$$\begin{aligned}
&\{\check{\psi}(d, f), \check{\sigma}(d, f), \check{m}(d, f)\} = \left\{ \frac{\sum_{s=1}^S g_s(d, f) \hat{\psi}_s(d, f)}{\sum_{s=1}^S g_s(d, f)}, \right. \\
&\quad \left. \frac{\sum_{s=1}^S g_s(d, f) \hat{\sigma}_s(d, f)}{\sum_{s=1}^S g_s(d, f)}, \frac{\sum_{s=1}^S g_s(d, f) \hat{m}_s(d, f)}{\sum_{s=1}^S g_s(d, f)} \right\}.
\end{aligned} \tag{28}$$

$$\begin{aligned}
\ell(\psi, \sigma, m) &= \sum_{s=1}^S \log \left( \frac{2 \left[ \frac{m\lambda}{\psi(\zeta^2-1)\zeta} \right]^{\frac{1}{2} \left( \frac{1}{\zeta^2-1} + m \right)}}{\Gamma(m)\Gamma\left(\frac{1}{\zeta^2-1}\right)} g_s^{\frac{1}{2} \left( \frac{1}{\zeta^2-1} + m \right) - 1} K_{\frac{1}{\zeta^2-1} - m} \left( 2 \left[ \frac{m\lambda g_s}{\psi(\zeta^2-1)\zeta} \right]^{\frac{1}{2}} \right) \right) \\
&= S \log(2) + \frac{S}{2} \left( \frac{1}{\zeta^2-1} + m \right) \log \left( \frac{m\lambda}{\psi(\zeta^2-1)\zeta} \right) - S \log(\Gamma(m)) - S \log \left( \Gamma \left( \frac{1}{\zeta^2-1} \right) \right) \\
&\quad + \left[ \frac{1}{2} \left( \frac{1}{\zeta^2-1} + m \right) - 1 \right] \sum_{s=1}^S \log(g_s) + \sum_{s=1}^S \log \left( K_{\frac{1}{\zeta^2-1} - m} \left( 2 \left[ \frac{m\lambda g_s}{\psi(\zeta^2-1)\zeta} \right]^{\frac{1}{2}} \right) \right)
\end{aligned} \tag{24}$$

**Algorithm 1** Proposed approximation process for numerically solving (25).

**input:** Tolerance  $\epsilon$ , step ratio  $\mu > 1$ ;

**output:** Approximate parameters  $\hat{\psi}_s(d, f)$ ,  $\hat{\sigma}_s(d, f)$ , and  $\hat{m}_s(d, f)$ ;

- 1: initialize  $\hat{\psi}_s(d, f) = 0$ ,  $\hat{\sigma}_s(d, f) = 0$ , and  $\hat{m}_s(d, f) = 0$ ;
- 2: **function** ApproxSubMLE( $d, f, g_s$ )
- 3:   **while**  $1/\tau > \epsilon$  **do**
- 4:     compute  $\psi^*, \sigma^*, m^*$  that jointly minimize  $\nu(\psi, \sigma, m)$  by implementing the conjugate gradient method, starting at the initialized point;
- 5:     update  $\hat{\psi}_s(d, f) = \psi^*$ ,  $\hat{\sigma}_s(d, f) = \sigma^*$ ,  $\hat{m}_s(d, f) = m^*$
- 6:     increment  $\tau = \mu\tau$ ;
- 7:   **end while**
- 8:   **return**  $\hat{\psi}_s(d, f)$ ,  $\hat{\sigma}_s(d, f)$ ,  $\hat{m}_s(d, f)$ ;
- 9: **end function**

The complete approximation process integrating all  $S$  random samples is summarized in Algorithm 2.

**Algorithm 2** Complete approximation process of the MLE method for estimating channel parameters for a specific space-frequency state.

**input:**  $S$  independently sampled internal channel power gain  $\{g_s\}$  for a specific space-frequency state  $(d, f)$ ;

**output:** Estimated optimal parameters  $\check{\psi}(d, f)$ ,  $\check{\sigma}(d, f)$ , and  $\check{m}(d, f)$ ;

- 1: **function** SubMLE( $d, f$ )
- 2:   initialize  $\check{\psi}(d, f) = 0$ ,  $\check{\sigma}(d, f) = 0$ ,  $\check{m}(d, f) = 0$ ;
- 3:    $\Sigma = \text{sum}(g_s)$ ;
- 4:   **for** each  $g_s$  in the sample set **do**
- 5:      $\{\hat{\psi}_s(d, f), \hat{\sigma}_s(d, f), \hat{m}_s(d, f)\} = \text{ApproxSubMLE}(d, f, g_s)$ ;
- 6:      $\rho = g_s/\Sigma$ ;
- 7:      $\check{\psi}(d, f) = \check{\psi}(d, f) + \rho * \hat{\psi}_s(d, f)$ ;
- 8:      $\check{\sigma}(d, f) = \check{\sigma}(d, f) + \rho * \hat{\sigma}_s(d, f)$ ;
- 9:      $\check{m}(d, f) = \check{m}(d, f) + \rho * \hat{m}_s(d, f)$ ;
- 10:   **end for**
- 11:   **return**  $\check{\psi}(d, f)$ ,  $\check{\sigma}(d, f)$ ,  $\check{m}(d, f)$ ;
- 12: **end function**

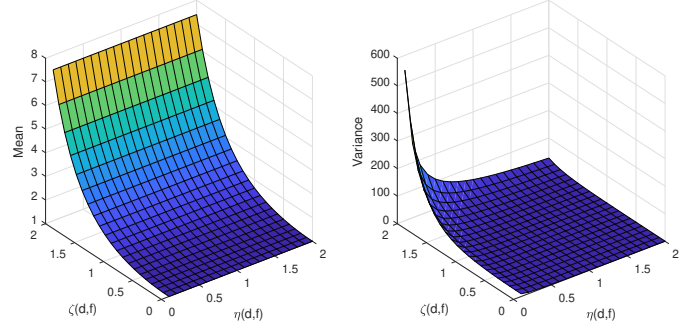


Fig. 2: Mean and variance of  $\delta_s(d, f)$  versus  $\zeta(d, f)$  and  $\eta(d, f)$ .

## V. NUMERICAL RESULTS AND DISCUSSION

In this section, we tailor a classic THz channel model proposed in [37] by introducing a gamma distributed random factor according to the multi-path effects shown in [23]. The tailored classic THz channel model is utilized to exemplify the parameter estimation procedure. To be clear, we denote the value of determinate internal channel power gain omitting the channel randomness as  $\dot{g}(d, f)$ , which is obtained from<sup>10</sup> [37]. To emulate the resultant randomness caused by propagation over the THz wireless channel on the internal channel power gain, we introduce a channel variation factor  $\delta_s(d, f)$ . The realization samples of random channel power gain incorporating stochastic factors can thereby be given as  $g_s(d, f) = \delta_s(d, f)\dot{g}(d, f)$ , which refers to the *tailored classic channel model*. Without loss of generality, we assume the channel variation factor to be gamma distributed with shape parameter  $\kappa_\delta(d, f) = \zeta(d, f)$  and  $\theta_\delta(d, f) = \exp(\eta(d, f)^2/2)/\zeta(d, f)$ . The mean and variance of  $\delta_s(d, f)$  versus  $\zeta(d, f)$  and  $\eta(d, f)$  are shown in Fig. 2.

However, due to the currently available data sets, we still cannot identify the exact values of  $\zeta(d, f)$  for different application scenarios, but we are able to approximate the range of  $\eta(d, f)$  to be [0.61, 1.80] for different transmission distances and radio frequencies, by inspecting the data of internal channel power loss in<sup>11</sup> [23]. The channel variation factor  $\delta_s(d, f)$  is assumed to be white and distance-independent for simplicity. Therefore, we let  $\zeta(d, f)$  and  $\eta(d, f)$  be predetermined constants for any transmission distance over the entire

<sup>10</sup>In fact, the data presented in [37] refers to the internal channel power loss, but since the gain is simply the reciprocal of the loss, the data of the internal channel power gain can be easily obtained.

<sup>11</sup>The approximation of this range is detailed in Appendix A.

THz band and plot the generated random realization samples of internal channel power gain in Fig. 3 for three cases with  $d = 0.1, 1, 10$  m.

#### A. Estimation and Verification of Free Channel Parameters

Based on the proposed randomization approach, we can obtain bundles of data samples of the internal channel power gain  $\{g_s(d, f)\}$  corresponding to different transmission distances and radio frequencies, when a set of random effects jointly apply. Processing these generated data samples by the MLE method stipulated in Section IV can yield the three estimated channel parameters  $\hat{\psi}(d, f)$ ,  $\hat{\sigma}(d, f)$ , and  $\hat{m}(d, f)$  for each space-frequency state  $(d, f)$ . To maintain an appropriate balance between computing efficiency and accuracy, for each space-frequency state, we collect  $S = 1000$  random samples for parameter estimation purposes. The estimated channel parameters over the low THz spectrum between 0.1 THz and 1 THz for different spreading loss exponents  $\alpha$  and transmission distances  $d$  are presented in Fig. 4.

Observing the estimated outcomes presented in Fig. 4, we can have a number of insights into the proposed compound THz channel model. First, from the data related to  $\hat{\psi}(d, f)$ , we can confirm that apart from the close proximity of several resonance frequencies, the molecular absorption over the low THz frequency spectrum (0.1 THz-1 THz) is negligible, especially when the transmission distance is less than 1 m. This is aligned with the theoretical derivations from physics [37]. Second, we can also confirm that the transmissions over the spectrum close to resonance frequencies are not possible, because of the sharp decreases in  $\hat{\psi}(d, f)$ ,  $\hat{\sigma}(d, f)$ , and  $\hat{m}(d, f)$ . Also, the spreading loss exponent  $\alpha$  only yields a significant impact on  $\hat{m}(d, f)$ , but has little impact on  $\hat{\psi}(d, f)$  and  $\hat{\sigma}(d, f)$ . This indicates the transferability of the outcomes of  $\hat{\psi}(d, f)$  and  $\hat{\sigma}(d, f)$  estimated under a specific value of  $\alpha$  to other cases with different values of  $\alpha$ . In terms of the effects of transmission distance  $d$  and radio frequency  $f$ , we can easily observe that  $\hat{\psi}(d, f)$  is distance- and frequency-dependent, which can be greatly varied by different  $d$  and  $f$ . On the other hand,  $\hat{\sigma}(d, f)$  is insensitive to the variations in both  $d$  and  $f$ , except when the radio frequency is close to the proximity of resonance frequencies.  $\hat{m}(d, f)$  is also distance- and frequency-dependent, which seems following the Friis' transmission law, except some random overshoots rendered by insufficient random realization samples.

Summarizing from the above observations, we find that  $m(d, f)$  is considerably affected by both of the spreading loss and multi-path fading. Meanwhile, a much higher  $m(d, f)$  in the THz band than that in the microwave band (usually less than 3.5) indicates that the multi-path fading is moderate and even trivial for THz radios [72]. The high value of  $m(d, f)$  is consistent with the experimental observation that THz radios present quasi-optical behaviors, and thereby the multi-path propagation links are much less and resolvable. The molecular absorption loss is mainly captured by  $\psi(d, f)$ , but also has impacts on  $\sigma(d, f)$  and  $m(d, f)$ ; shadowing is reflected by  $\sigma(d, f)$ , which is independent of transmission distance and radio frequency, except in proximity of resonance frequencies.

Once the radio frequency is close to the proximity of resonance frequencies, the shadowing effect becomes drastically severe, and a low  $\sigma(d, f)$  is resulted, which is analogous to existing an invisible 'THz wall' [18]. In addition, in most cases, we have  $\frac{1}{\exp(\sigma(d, f)^2) - 1} \ll m(d, f)$ , implying that the severity of shadowing is much higher than that of multi-path fading.

With the estimated channel parameters  $\hat{\psi}(d, f)$ ,  $\hat{\sigma}(d, f)$ , and  $\hat{m}(d, f)$ , we can in turn refer to (10) to formulate the analytical CDF of the internal channel power gain  $\tilde{g}(d, f)$  for a given space-frequency state  $(d, f)$ . Also, through the  $S$  random realization samples  $\{g_s(d, f)\}$ , we can construct the empirical CDF by utilizing the non-parametric Kaplan-Meier estimation [73]. By comparing the analytical and empirical CDFs and checking whether they match each other, we are able to judge whether the compound THz channel model based on the estimated channel parameters  $\hat{\psi}(d, f)$ ,  $\hat{\sigma}(d, f)$ , and  $\hat{m}(d, f)$  is capable of accurately capturing the traits of realistic THz wireless channels and maintaining the fidelity. For a set of representative space-frequency states, we plot the empirical and analytical CDFs of the internal channel power gain  $\tilde{g}(d, f)$  in Fig. 5 (the x-axis scales of subplots in this figure are varied so that the key distribution regions can be clearly shown). From Fig. 5, we verify that the estimated channel parameters  $\hat{\psi}(d, f)$ ,  $\hat{\sigma}(d, f)$ , and  $\hat{m}(d, f)$  by the MLE method in (23) can accurately capture the statistical traits of THz wireless channels. It should be noted that there are some tiny mismatches between the analytical CDF and empirical CDF sometimes, which indicates that the parameter estimation is not always perfectly accurate. This is mainly because the THz band is highly dynamic and frequency-selective, where the path loss experiences a large number of steep rises and steep drops. The accuracy of the proposed estimation method varies with the communication scenarios. However, the compound THz channel model based on the estimated channel parameters still demonstrates good accuracy in general. Therefore, we can rely on the proposed model to simulate THz communication systems with different space-frequency states and verify the outage performance analysis in the following.

#### B. Verification of Outage Performance Analysis

Based on the verified estimated channel parameters, we can further verify the exact and asymptotic outage performance analysis derived in Section III. The outage probability is related to the transmitted data size, which depends on the number of the transmitted packets. Observing from Fig. 6, we can see that the outage probability decreases as  $\lambda_p$  decreases. This is because the packet number follows a Poisson distribution with an average rate  $\lambda_p$ . Intuitively, a higher  $\lambda_p$  indicates more packets needed to be transmitted, which yields a longer transmission delay and thereby a higher outage probability. Moreover, since a lower delay threshold implies that the system experiences a better channel situation, it is aligned with our expectation that the system with a larger  $\varepsilon$  outperforms the one with a smaller  $\varepsilon$ . Moreover, the asymptotic results for the outage probability obtained in Section III-C can accurately match the simulation and analysis in the low average packet arrival rate regime.

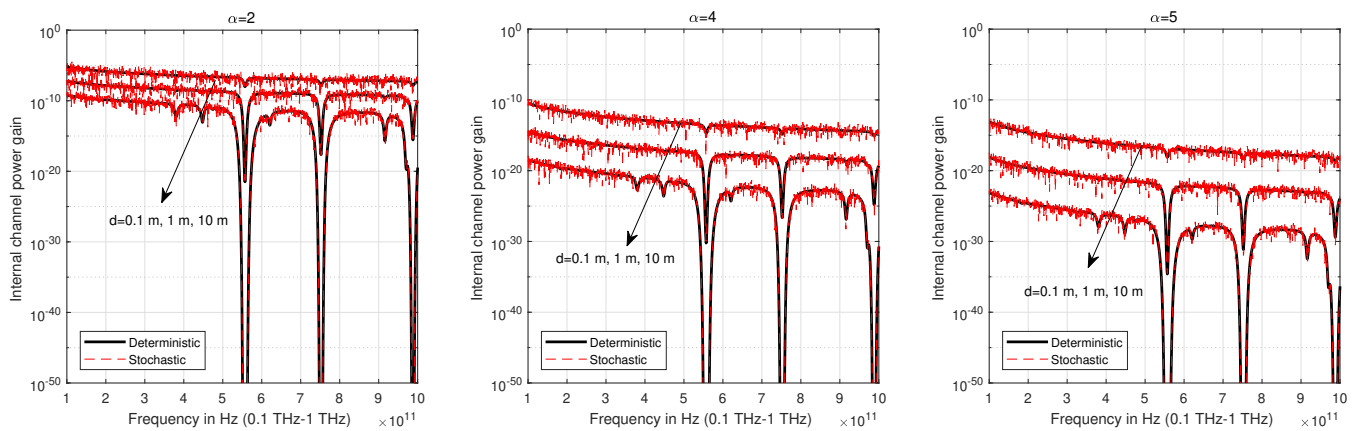


Fig. 3: Internal channel power gain versus radio frequency for cases with different transmission distances, given  $\zeta(d, f) = 1$  and  $\eta(d, f) = 1$ .

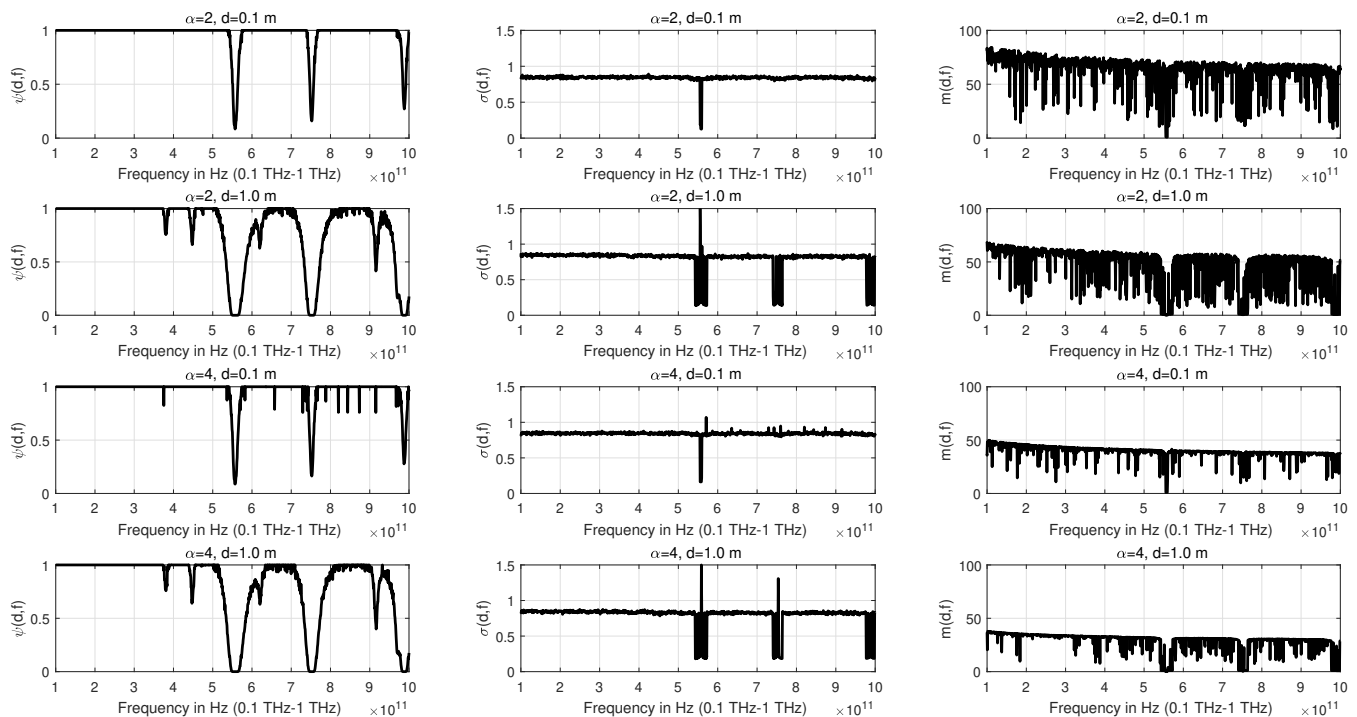


Fig. 4: Estimated channel parameters  $\hat{\psi}(d, f)$ ,  $\hat{\sigma}(d, f)$ , and  $\hat{m}(d, f)$  with different spreading loss exponents and transmission distances, given  $S = 1000$ ,  $\zeta(d, f) = 1$  and  $\eta(d, f) = 1$ .

In Fig. 7, we show the impact of the size length of each transmitted packet. As we can observe, the outage probability decreases as  $L$  decreases since the total number of transmitted bits decreases. Assuming the same number of packets to be transmitted, this yields a shorter transmission delay and thereby a lower outage probability. It plays the same negative role as the average packet arrival rate  $\lambda_p$ . One can also observe that the outage probability saturates in the high transmitting PSD regime, which perfectly matches with the floor derived in Section III-C. This behavior stems from the fact that noise power at the receiver increases as the transmitting power increases.

Comparing the three cases shown in Fig. 6, we can further observe that the path loss factor and the communication distance both have negative impacts on system performance.

However, since the data transmissions of THz communication systems occur within a short transmission distance, the outage performance is not significantly impaired by the increase in the path loss factor from 2 to 4, while it is greatly degraded when the communication distance increases from 0.1 m to 1 m. Meanwhile, these simulation results show that the derived outage probabilities with the estimated channel parameters are in a tight agreement with their empirical counterparts, which verifies the correctness of our derivations for outage performance in Section III.

## VI. CONCLUSION

To attract the attention of the PHY communication research community and accelerate the research progress on THz communications, we analyzed the outage performance

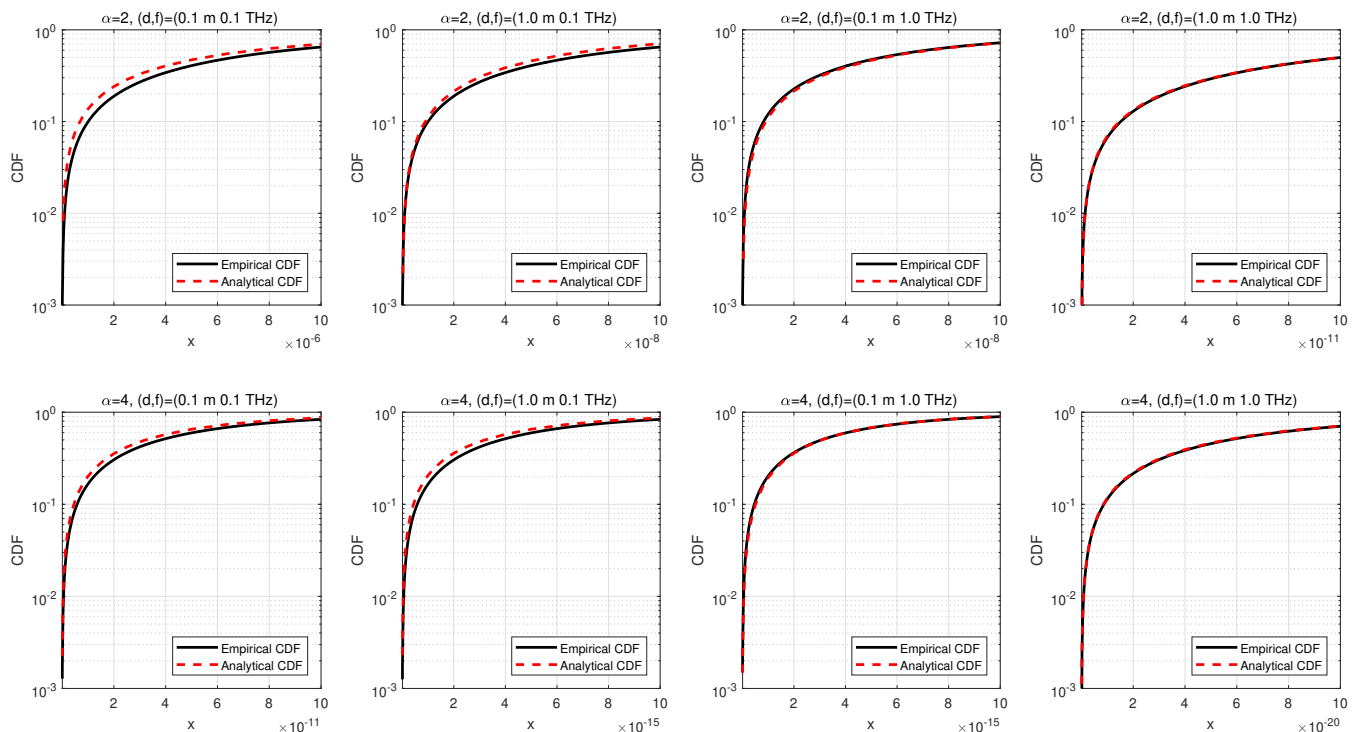


Fig. 5: Comparison between the empirical and analytical CDFs of the internal channel power gain, given  $\zeta(d, f) = 1$  and  $\eta(d, f) = 1$  (the x-axis scales of subplots are varied so that the key distribution regions can be clearly shown).

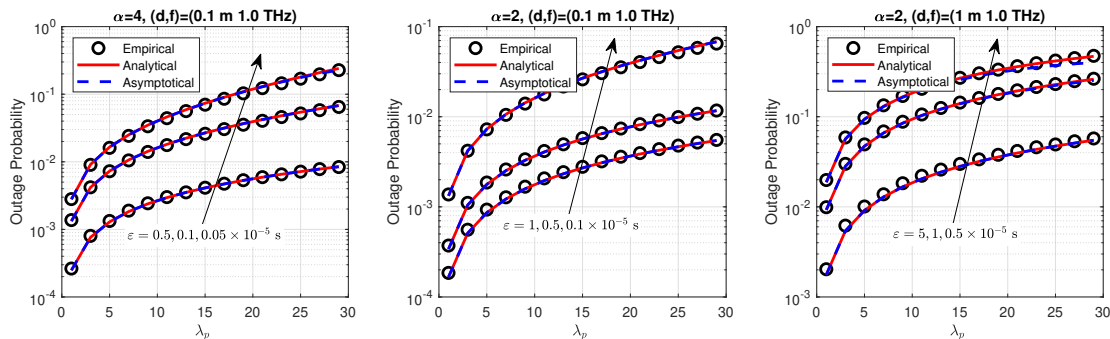


Fig. 6: Outage probability versus outage threshold with average packet arrival rate with different outage threshold, given  $L = 10$  bits,  $\zeta(d, f) = 1$ , and  $\eta(d, f) = 1$ .

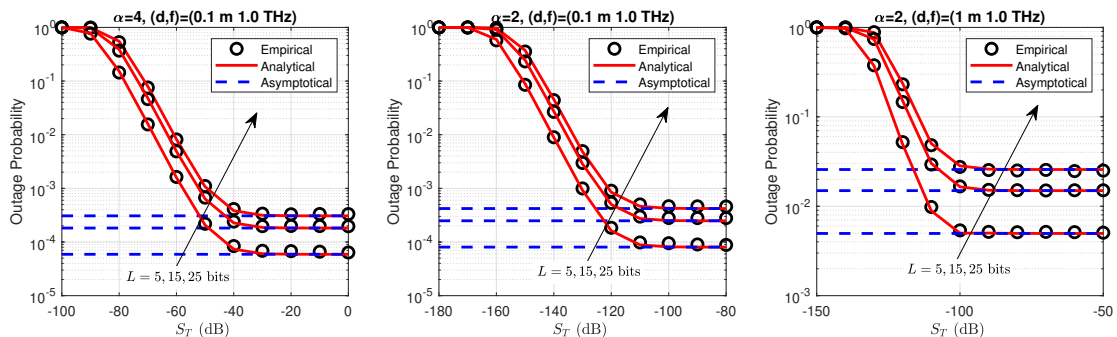


Fig. 7: Outage probability versus transmitting PSD with different packet length, given  $\lambda_p = 10$ ,  $\varepsilon = 10^{-4}$  s,  $\zeta(d, f) = 1$ , and  $\eta(d, f) = 1$ .

for THz wireless systems based on the tailored compound channel model in this paper. In this compound model, most determinate and stochastic effects, including spreading loss, molecular absorption loss, shadowing, and multi-path fading,

are jointly considered via a joint distribution depending on three free parameters. The PDF, CDF, and outage probability derived from the tailored compound model are given in closed-form expressions, which indicate an appropriate equilibrium

between mathematical tractability and the fidelity of realistic THz channels. In addition, we leveraged the MLE method to design a channel parameter estimation approach for the proposed compound channel model and obtained the estimates in a computational-efficient manner. These estimates can be directly reused by researchers to model THz communication systems. The derived analytical results were verified by numerical simulations using Monte Carlo methods. By the simplicity and the mathematical tractability of the outage performance presented in this paper, it is expected to considerably facilitate advanced analyses and optimization for THz communication systems.

#### APPENDIX A

##### APPROXIMATION OF THE RANGE OF $\eta(d, f)$

Denote the difference between the channel power loss of the LoS case and the average channel power loss of the multi-path case in dB as  $\Delta(d, f)$ , which is distance- and frequency-dependent. Based on the relation between loss and gain, as well as the relation between linear and decibel units, we can easily derive the following relation:  $\Delta(d, f) = 10 \log_{10}(1/\dot{g}(d, f)) - 10 \log_{10}(1/\mathbb{E}\{g_s(d, f)\})$ , by which we can further deduce  $\mathbb{E}\{\delta_s(d, f)\} = \mathbb{E}\{g_s(d, f)\}/\dot{g}(d, f) = 10^{\Delta(d, f)/10}$ . According to the assumption that  $\delta_s(d, f)$  is gamma distributed with shape parameter  $\kappa_\delta(d, f) = \zeta(d, f)$  and  $\theta_\delta(d, f) = \exp(\eta(d, f)^2/2)$ , the expected value of channel variation factor  $\delta_s(d, f)$  can be determined as  $\mathbb{E}\{\delta_s(d, f)\} = \kappa_\delta(d, f)\theta_\delta(d, f) = \exp(\eta(d, f)^2/2)$ , which directly leads to

$$\eta(d, f) = \left( \frac{\Delta(d, f)}{5} \log(10) \right)^{\frac{1}{2}}. \quad (29)$$

Inspecting the data presented in Fig. 4 of [23],  $\Delta(d, f)$  ranges from 0.8 dB to 7 dB depending on the transmission distance and radio frequency. Substituting the range of  $\Delta(d, f)$  into (29) directly yields the range of  $\eta(d, f)$  to be [0.61, 1.80].

#### ACKNOWLEDGMENT

The authors thank Prof. Josep M. Jornet with Northeastern University, USA, and Prof. Chong Han with Shanghai Jiao Tong University, China, for providing programs and data of the THz channel, which are used in this paper for verification purposes and accelerate our research progress.

#### REFERENCES

- [1] S. Dang, O. Amin, B. Shihada, and M.-S. Alouini, "What should 6G be?" *Nature Electronics*, vol. 3, no. 1, pp. 20–29, 2020.
- [2] M. Dohler, R. W. Heath, A. Lozano, C. B. Papadias, and R. A. Valenzuela, "Is the PHY layer dead?" *IEEE Communications Magazine*, vol. 49, no. 4, pp. 159–165, Apr. 2011.
- [3] Z. Ding, X. Lei, G. K. Karagiannidis, R. Schober, J. Yuan, and V. K. Bhargava, "A survey on non-orthogonal multiple access for 5G networks: Research challenges and future trends," *IEEE Journal on Selected Areas in Communications*, vol. 35, no. 10, pp. 2181–2195, Oct. 2017.
- [4] E. Basar, M. Wen, R. Mesleh, M. Di Renzo, Y. Xiao, and H. Haas, "Index modulation techniques for next-generation wireless networks," *IEEE Access*, vol. 5, pp. 16 693–16 746, 2017.
- [5] H. Elayan, O. Amin, B. Shihada, R. M. Shubair, and M.-S. Alouini, "Terahertz band: The last piece of RF spectrum puzzle for communication systems," *IEEE Open Journal of the Communications Society*, vol. 1, pp. 1–32, 2020.
- [6] D. He, B. Ai, K. Guan, L. Wang, Z. Zhong, and T. Kurner, "The design and applications of high-performance ray-tracing simulation platform for 5G and beyond wireless communications: A tutorial," *IEEE Communications Surveys Tutorials*, vol. 21, no. 1, pp. 10–27, 2019.
- [7] K. M. S. Huq, S. A. Busari, J. Rodriguez, V. Frascolla, W. Bazzi, and D. C. Sicker, "Terahertz-enabled wireless system for beyond-5G ultra-fast networks: A brief survey," *IEEE Network*, vol. 33, no. 4, pp. 89–95, July 2019.
- [8] H. Sariyeddeen, M.-S. Alouini, and T. Y. Al-Naffouri, "An overview of signal processing techniques for terahertz communications," *arXiv preprint arXiv:2005.13176*, 2020.
- [9] I. F. Akyildiz and J. M. Jornet, "The Internet of nano-things," *IEEE Wireless Communications*, vol. 17, no. 6, pp. 58–63, Dec. 2010.
- [10] H. Song and T. Nagatsuma, "Present and future of terahertz communications," *IEEE Transactions on Terahertz Science and Technology*, vol. 1, no. 1, pp. 256–263, Sept. 2011.
- [11] I. F. Akyildiz, J. M. Jornet, and C. Han, "TeraNets: Ultra-broadband communication networks in the terahertz band," *IEEE Wireless Communications*, vol. 21, no. 4, pp. 130–135, Aug. 2014.
- [12] I. F. Akyildiz, J. M. Jornet, and C. Han, "Terahertz band: Next frontier for wireless communications," *Physical Communication*, vol. 12, pp. 16–32, 2014.
- [13] T. Nagatsuma, G. Ducournau, and C. C. Renaud, "Advances in terahertz communications accelerated by photonics," *Nature Photonics*, vol. 10, no. 6, p. 371, 2016.
- [14] Z. Hossain, Q. Xia, and J. M. Jornet, "TeraSim: An ns-3 extension to simulate terahertz-band communication networks," *Nano Communication Networks*, vol. 17, pp. 36–44, 2018.
- [15] K. Guan, G. Li, T. Kurner, A. F. Molisch, B. Peng, R. He, B. Hui, J. Kim, and Z. Zhong, "On millimeter wave and THz mobile radio channel for smart rail mobility," *IEEE Transactions on Vehicular Technology*, vol. 66, no. 7, pp. 5658–5674, 2017.
- [16] K. Guan, D. He, B. Ai, D. W. Matolak, Q. Wang, Z. Zhong, and T. Kurner, "5-GHz obstructed vehicle-to-vehicle channel characterization for Internet of Intelligent Vehicles," *IEEE Internet of Things Journal*, vol. 6, no. 1, pp. 100–110, 2019.
- [17] K. Guan, B. Peng, D. He, J. M. Eckhardt, S. Rey, B. Ai, Z. Zhong, and T. Kurner, "Channel characterization for intra-wagon communication at 60 and 300 GHz bands," *IEEE Transactions on Vehicular Technology*, vol. 68, no. 6, pp. 5193–5207, 2019.
- [18] C. M. Armstrong, "The truth about terahertz," *IEEE Spectrum*, vol. 49, no. 9, pp. 36–41, Sept. 2012.
- [19] K. Tsujimura, K. Umehayashi, J. Kokkonen, J. Lehtomäki, and Y. Suzuki, "A causal channel model for the terahertz band," *IEEE Transactions on Terahertz Science and Technology*, vol. 8, no. 1, pp. 52–62, Jan. 2018.
- [20] V. Petrov, D. Moltchanov, and Y. Koucheryavy, "Interference and SINR in dense terahertz networks," in *Proc. IEEE VTC Fall*, Boston, MA, USA, Sept. 2015, pp. 1–5.
- [21] J. Kokkonen, J. Lehtomäki, and M. Juntti, "Stochastic geometry analysis for mean interference power and outage probability in THz networks," *IEEE Transactions on Wireless Communications*, vol. 16, no. 5, pp. 3017–3028, May 2017.
- [22] J. Kokkonen, J. Lehtomäki, and M. Juntti, "A discussion on molecular absorption noise in the terahertz band," *Nano communication networks*, vol. 8, pp. 35–45, 2016.
- [23] C. Han and Y. Chen, "Propagation modeling for wireless communications in the terahertz band," *IEEE Communications Magazine*, vol. 56, no. 6, pp. 96–101, June 2018.
- [24] I. F. Akyildiz, C. Han, and S. Nie, "Combating the distance problem in the millimeter wave and terahertz frequency bands," *IEEE Communications Magazine*, vol. 56, no. 6, pp. 102–108, June 2018.
- [25] A. Hirata and M. Yaita, "Ultrafast terahertz wireless communications technologies," *IEEE Transactions on Terahertz Science and Technology*, vol. 5, no. 6, pp. 1128–1132, 2015.
- [26] C. Han and I. F. Akyildiz, "Distance-aware bandwidth-adaptive resource allocation for wireless systems in the terahertz band," *IEEE Transactions on Terahertz Science and Technology*, vol. 6, no. 4, pp. 541–553, July 2016.
- [27] V. Petrov, A. Pyattaev, D. Moltchanov, and Y. Koucheryavy, "Terahertz band communications: Applications, research challenges, and standardization activities," in *Proc. IEEE ICUMT*, Lisbon, Portugal, Oct. 2016, pp. 183–190.
- [28] K. Guan, B. Peng, D. He, J. M. Eckhardt, S. Rey, B. Ai, Z. Zhong, and T. Kurner, "Measurement, simulation, and characterization of train-to-infrastructure inside-station channel at the terahertz band," *IEEE*

- Transactions on Terahertz Science and Technology*, vol. 9, no. 3, pp. 291–306, 2019.
- [29] Z. Chen, X. Ma, B. Zhang, Y. Zhang, Z. Niu, N. Kuang, W. Chen, L. Li, and S. Li, “A survey on terahertz communications,” *China Communications*, vol. 16, no. 2, pp. 1–35, Feb. 2019.
- [30] S. Priebe and T. Kurner, “Stochastic modeling of THz indoor radio channels,” *IEEE Transactions on Wireless Communications*, vol. 12, no. 9, pp. 4445–4455, Sept. 2013.
- [31] V. Petrov, M. Komarov, D. Moltchanov, J. M. Jornet, and Y. Koucheryavy, “Interference and SINR in millimeter wave and terahertz communication systems with blocking and directional antennas,” *IEEE Transactions on Wireless Communications*, vol. 16, no. 3, pp. 1791–1808, 2017.
- [32] V. Petrov, J. Kokkonen, D. Moltchanov, J. Lehtomaki, Y. Koucheryavy, and M. Juntti, “Last meter indoor terahertz wireless access: Performance insights and implementation roadmap,” *IEEE Communications Magazine*, vol. 56, no. 6, pp. 158–165, 2018.
- [33] I. M. Kostic, “Analytical approach to performance analysis for channel subject to shadowing and fading,” *IEEE Proceedings - Communications*, vol. 152, no. 6, pp. 821–827, Dec. 2005.
- [34] S. Al-Ahmadi, “The gamma-gamma signal fading model: A survey [wireless corner],” *IEEE Antennas and Propagation Magazine*, vol. 56, no. 5, pp. 245–260, 2014.
- [35] I. Trigui, P. D. Diamantoulakis, S. Affes, and G. K. Karagiannidis, “Shadowed FSO/mmWave systems with interference,” *IEEE Transactions on Communications*, vol. 67, no. 9, pp. 6256–6267, 2019.
- [36] C. Li, H. Wang, J. Yao, and S. Du, “Success probability of millimeter wave cellular networks under the Nakagami-lognormal fading channel,” in *Proc. IEEE ICTC*, Jeju Island, South Korea, 2019, pp. 189–192.
- [37] J. M. Jornet and I. F. Akyildiz, “Channel modeling and capacity analysis for electromagnetic wireless nanonetworks in the terahertz band,” *IEEE Transactions on Wireless Communications*, vol. 10, no. 10, pp. 3211–3221, Oct. 2011.
- [38] A. Moldovan, M. A. Ruder, I. F. Akyildiz, and W. H. Gerstacker, “LOS and NLOS channel modeling for terahertz wireless communication with scattered rays,” in *Proc. IEEE Globecom Workshops (GC Wkshps)*, Austin, TX, USA, 2014, pp. 388–392.
- [39] S. Shah, M. Ashraf, N. Saeed, T. Jan, R. Khalil, M. I. Babar, G. Ahmad, and S. W. Shah, “Path loss model for future terahertz (THz) wireless communication systems,” *Proceedings of the Pakistan Academy of Sciences: A. Physical and Computational Sciences*, vol. 56, no. 2, pp. 55–65, 2019.
- [40] Bile Peng, S. Rey, and T. Kürner, “Channel characteristics study for future indoor millimeter and submillimeter wireless communications,” in *Proc. IEEE European Conference on Antennas and Propagation (EuCAP)*, Davos, Switzerland, 2016, pp. 1–5.
- [41] A. R. Ekti, A. Boyaci, A. Alparslan, I. Unal, S. Yarkan, A. Gorcin, H. Arslan, and M. Uysal, “Statistical modeling of propagation channels for terahertz band,” in *Proc. IEEE CSCN*, Helsinki, Finland, Sept. 2017, pp. 275–280.
- [42] F. Sheikh, D. Lessy, and T. Kaiser, “A novel ray-tracing algorithm for non-specular diffuse scattered rays at terahertz frequencies,” in *Proc. IEEE International Workshop on Mobile Terahertz Systems (IWMTS)*, Duisburg, Germany, 2018, pp. 1–6.
- [43] F. Sheikh, M. Alissa, A. Zahid, Q. H. Abbasi, and T. Kaiser, “Atmospheric attenuation analysis in indoor THz communication channels,” in *Proc. IEEE International Symposium on Antennas and Propagation and USNC-URSI Radio Science Meeting*, Atlanta, GA, USA, 2019, pp. 2137–2138.
- [44] Y. Choi, J.-W. Choi, and J. M. Cioffi, “A geometric-statistic channel model for THz indoor communications,” *Journal of Infrared, Millimeter, and Terahertz Waves*, vol. 34, no. 7–8, pp. 456–467, 2013.
- [45] C. Han, A. O. Bicen, and I. F. Akyildiz, “Multi-ray channel modeling and wideband characterization for wireless communications in the terahertz band,” *IEEE Transactions on Wireless Communications*, vol. 14, no. 5, pp. 2402–2412, May 2015.
- [46] Z. Hossain, C. Mollica, and J. M. Jornet, “Stochastic multipath channel modeling and power delay profile analysis for terahertz-band communication,” in *Proceedings of the 4th ACM International Conference on Nanoscale Computing and Communication*, 2017, pp. 1–7.
- [47] S. Kim and A. Zajić, “Statistical modeling and simulation of short-range device-to-device communication channels at sub-THz frequencies,” *IEEE Transactions on Wireless Communications*, vol. 15, no. 9, pp. 6423–6433, 2016.
- [48] K. Tekbilyk, E. Ulusoy, A. R. Ekti, S. Yarkan, T. Baykas, A. Gorcin, and G. K. Kurt, “Statistical channel modeling for short range line-of-sight terahertz communication,” in *Proc. IEEE Annual International Symposium on Personal, Indoor and Mobile Radio Communications (PIMRC)*, Istanbul, Turkey, 2019, pp. 1–5.
- [49] D. He, K. Guan, A. Fricke, B. Ai, R. He, Z. Zhong, A. Kasamatsu, I. Hosako, and T. Kurner, “Stochastic channel modeling for kiosk applications in the terahertz band,” *IEEE Transactions on Terahertz Science and Technology*, vol. 7, no. 5, pp. 502–513, Sept. 2017.
- [50] P. M. Shankar, “Outage probabilities in shadowed fading channels using a compound statistical model,” *IEE Proceedings - Communications*, vol. 152, no. 6, pp. 828–832, 2005.
- [51] P. S. Bithas, N. C. Sagiias, P. T. Mathiopoulos, G. K. Karagiannidis, and A. A. Rontogiannis, “On the performance analysis of digital communications over generalized-K fading channels,” *IEEE Communications Letters*, vol. 10, no. 5, pp. 353–355, 2006.
- [52] J. Proakis and M. Salehi, *Digital Communications*. McGraw-Hill, 2008.
- [53] T. S. Rappaport, *Wireless Communications: Principles And Practice*. Pearson Education, 2010.
- [54] J. M. Jornet and I. F. Akyildiz, “Channel modeling and capacity analysis for electromagnetic wireless nanonetworks in the terahertz band,” *IEEE Transactions on Wireless Communications*, vol. 10, no. 10, pp. 3211–3221, 2011.
- [55] —, “Femtosecond-long pulse-based modulation for terahertz band communication in nanonetworks,” *IEEE Transactions on Communications*, vol. 62, no. 5, pp. 1742–1754, 2014.
- [56] M. Pierobon, J. M. Jornet, N. Akkari, S. Almasri, and I. F. Akyildiz, “A routing framework for energy harvesting wireless nanosensor networks in the terahertz band,” *Wireless networks*, vol. 20, no. 5, pp. 1169–1183, 2014.
- [57] P. Boronin, V. Petrov, D. Moltchanov, Y. Koucheryavy, and J. M. Jornet, “Capacity and throughput analysis of nanoscale machine communication through transparency windows in the terahertz band,” *Nano Communication Networks*, vol. 5, no. 3, pp. 72–82, 2014.
- [58] G. Mao, B. D. Anderson, and B. Fidan, “Path loss exponent estimation for wireless sensor network localization,” *Computer Networks*, vol. 51, no. 10, pp. 2467–2483, 2007.
- [59] N. A. Tultul, S. Farha, S. S. Hossain, M. A. Hossain, and S. R. Sabuj, “Device-to-device communication in terahertz frequency band: Enhancement of energy efficiency,” in *2020 IEEE REGION 10 CONFERENCE (TENCON)*. IEEE, 2020, pp. 117–122.
- [60] H. Xing and S. Hakola, “The investigation of power control schemes for a device-to-device communication integrated into OFDMA cellular system,” in *21st Annual IEEE International Symposium on Personal, Indoor and Mobile Radio Communications*. IEEE, 2010, pp. 1775–1780.
- [61] A.-A. A. Boulogeorgos and A. Alexiou, “Outage probability analysis of THz relaying systems,” in *2020 IEEE 31st Annual International Symposium on Personal, Indoor and Mobile Radio Communications*. IEEE, 2020, pp. 1–7.
- [62] E. N. Papatotiriou, A.-A. A. Boulogeorgos, and A. Alexiou, “Performance analysis of THz wireless systems in the presence of antenna misalignment and phase noise,” *IEEE Communications Letters*, vol. 24, no. 6, pp. 1211–1215, 2020.
- [63] A.-A. A. Boulogeorgos and A. Alexiou, “Performance evaluation of the initial access procedure in wireless THz systems,” in *2019 16th International Symposium on Wireless Communication Systems (ISWCS)*. IEEE, 2019, pp. 422–426.
- [64] A. A. Joshi, P. Bhardwaj, and S. Zafaruddin, “Terahertz wireless transmissions with maximal ratio combining over fluctuating two-ray fading,” *arXiv preprint arXiv:2108.01698*, 2021.
- [65] J. Zhang, W. Zeng, X. Li, Q. Sun, and K. P. Peppas, “New results on the fluctuating two-ray model with arbitrary fading parameters and its applications,” *IEEE Transactions on Vehicular Technology*, vol. 67, no. 3, pp. 2766–2770, 2018.
- [66] H. Sariahmedeen, M.-S. Alouini, and T. Y. Al-Naffouri, “Terahertz-band ultra-massive spatial modulation MIMO,” *IEEE Journal on Selected Areas in Communications*, vol. 37, no. 9, pp. 2040–2052, 2019.
- [67] X. Wang, P. Wang, M. Ding, Z. Lin, F. Lin, B. Vucetic, and L. Hanzo, “Performance analysis of terahertz unmanned aerial vehicular networks,” *IEEE Transactions on Vehicular Technology*, vol. 69, no. 12, pp. 16330–16335, 2020.
- [68] A. T. Hoang and M. Motani, “Buffer and channel adaptive modulation for transmission over fading channels,” in *Proc. ICC.*, vol. 4, Anchorage, AK, USA, 2003, pp. 2748–2752.
- [69] I. S. Gradshteyn and I. M. Ryzhik, *Table of Integrals, Series, and Products*. Academic Press, 2014.
- [70] R. Millar, *Maximum Likelihood Estimation and Inference: With Examples in R, SAS and ADMB*, ser. Statistics in Practice. Wiley, 2011.

- [71] Y. Nesterov, *Lectures on convex optimization*. Springer, 2018, vol. 137.
- [72] P. Shankar, "Outage analysis in wireless channels with multiple interferers subject to shadowing and fading using a compound pdf model," *AEU-International Journal of Electronics and Communications*, vol. 61, no. 4, pp. 255–261, 2007.
- [73] E. L. Kaplan and P. Meier, "Nonparametric estimation from incomplete observations," *Journal of the American statistical association*, vol. 53, no. 282, pp. 457–481, 1958.